

Certifying entanglement of spins on surfaces using ESR-STM

Y. del Castillo^{1,2} and J. Fernández-Rossier^{1,*}

¹*International Iberian Nanotechnology Laboratory (INL), Av. Mestre José Veiga, 4715-330 Braga, Portugal*

²*Centro de Física das Universidades do Minho e do Porto, Universidade do Minho, Campus de Gualtar, 4710-057 Braga, Portugal*

 (Received 21 December 2022; revised 29 June 2023; accepted 14 August 2023; published 7 September 2023)

We propose a protocol to certify the presence of entanglement in artificial on-surface atomic and molecular spin arrays using electron spin resonance carried by scanning tunnel microscopy (ESR-STM). We first generalize the theorem that relates global spin susceptibility as an entanglement witness to the case of anisotropic Zeeman interactions, relevant for surfaces. We then propose a method to measure the spin susceptibilities of surface-spin arrays combining ESR-STM with atomic manipulation. Our calculations show that entanglement can be certified in antiferromagnetically coupled spin dimers and trimers with state-of-the-art ESR-STM magnetometry.

DOI: [10.1103/PhysRevB.108.115413](https://doi.org/10.1103/PhysRevB.108.115413)

I. INTRODUCTION

Very much like electricity and magnetism, quantum entanglement is a naturally occurring phenomena. Entanglement lies at the heart of the most intriguing aspects of quantum mechanics [1], such as quantum teleportation [2–4], nonlocality, and the emergence of exotic quantum states of matter [5]. The notion that quantum entanglement is also a resource that can be exploited is at the cornerstone of the fields of quantum computing [6], quantum sensing [7], and quantum communications [8]. In order to harness quantum entanglement, it seems imperative to develop tools to probe it [9]. This can be particularly challenging at the nanoscale [10].

Quantum entanglement is predicted to occur spontaneously in interacting spin systems [11,12], going from small clusters to crystals. In the last few decades, tools to create and probe artificial spin arrays based on both magnetic atoms and molecules on surface have been developed [13–15]. There is now a growing interest in the exploitation of quantum behavior of this class of systems [16,17]. Surface-spin artificial arrays can display exotic quantum magnetism phenomena, including spin fractionalization in $S = 1$ Haldane chains [18], resonant valence bond states in spin plaquettes [19], and quantum criticality [20] that are known to host entangled states. However, the lack of an on-surface single-shot readout method, available in other platforms [21,22], prevents the implementation of quantum state tomography that would make it possible to quantify entanglement.

Here we tackle this important problem and we propose a protocol to certify the presence of entanglement on artificial arrays of surface spins, leveraging on state-of-the-art experimental techniques for spins on surfaces. The approach relies on two ideas. First, it was both proposed [23–25] and demonstrated experimentally [24,26] in bulk systems, that the trace of the finite-temperature spin susceptibility matrix can be used

as an entanglement witness (EW) regardless of the type of entanglement. Second, the development [27] of single-atom electron spin resonance using scanning tunneling microscopy (ESR-STM) that, combined with atomic manipulation, has made it possible to carry out absolute magnetometry [28,29] of surface spins. As illustrated in the scheme of Fig. 1, the magnetic field created by the different quantum states of the surface spins can be measured by an ESR-STM active atomic spin sensor placed nearby. The accurate determination of the height of the corresponding peaks and their shift makes it possible to pull out both their occupation and magnetic moment, which permits one to determine the finite-temperature spin susceptibility, if interactions between the array and the substrate are negligible compared with the interactions between the surface spins.

The global spin susceptibility is defined as the linear coefficient that relates the external magnetic field to the average total magnetization

$$\langle M_\alpha \rangle = \chi_\alpha B_\alpha, \quad (1)$$

where $\langle \cdot \rangle$ stands for statistical average in thermal equilibrium, and

$$M_\alpha = \sum_i m_\alpha^i = -\mu_B \sum_i g_\alpha S_\alpha^i, \quad (2)$$

where $\alpha = x, y, z$ labels the principal axes that diagonalize the susceptibility tensor and i labels the site in a given spin lattice.

II. SPINS SUSCEPTIBILITY AS ENTANGLEMENT WITNESS

The interaction between the spins of interest and the external field is given by $\mathcal{H}_1 = -\sum_\alpha M_\alpha B_\alpha$. For spin-rotational invariant Hamiltonians that commute with the Zeeman operator, $[\mathcal{H}_0, \mathcal{H}_1] = 0$, the spin susceptibility and the statistical variance of the total magnetization, ΔM_α^2 , are related by [23,30]

$$\chi_\alpha = \beta \Delta M_\alpha^2 = \beta \left[\sum_{i,j} \langle m_\alpha^i m_\alpha^j \rangle - \left(\sum_i \langle m_\alpha^i \rangle \right)^2 \right], \quad (3)$$

*On permanent leave from Departamento de Física Aplicada, Universidad de Alicante, 03690 San Vicente del Raspeig, Spain; joaquin.fernandez-rossier@inl.int

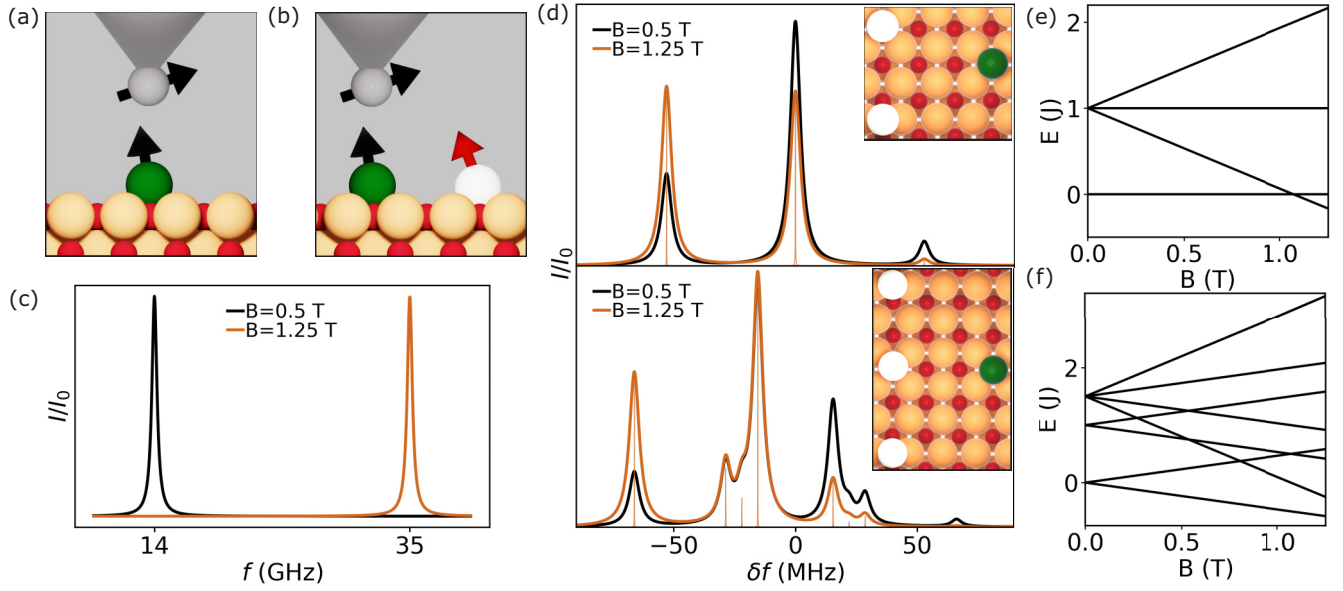


FIG. 1. Scheme of the proposed ESR-STM experimental protocol. (a) Characterization of the bare resonance frequency f_0 of the sensor. (b) Determination of the g coefficients of a single unit (atom) of the on-surface spin array. (c) ESR-STM readout of the bare sensor at two different fields. (d) ESR-STM readouts of a sensor nearby an antiferromagnetically coupled dimer (top) and a trimer (bottom), with $J = 124\mu\text{eV}$ and $T = 1$ K, using different magnetic fields that lead to different occupations of the states. (e) and (f) Energy spectra of the dimer and trimer as a function of B .

where $\beta = \frac{1}{k_B T}$. The variance for an isolated spin satisfies $\sum_{\alpha} g_{\alpha}^2 \Delta S_{\alpha}^2 \geq g_{\min}^2 S$ where $g_{\min} = \text{Min}(g_x, g_y, g_z)$. For a multispin system it has been shown [32] that, for nonentangled states, the variance of the total magnetization is at least as large as the sum over variances of individual magnetizations. We thus can write the equation

$$\begin{aligned} \text{Tr } \chi &= \sum_{\alpha} \chi_{\alpha} = \chi_x + \chi_y + \chi_z \\ &= \beta \sum_{\alpha} \left[\sum_{i,j} \langle m_{\alpha}^i m_{\alpha}^j \rangle - \left(\sum_i \langle m_{\alpha}^i \rangle \right)^2 \right] \geq \frac{g_{\min}^2 \mu_B^2 S}{k_B T} N \end{aligned} \quad (4)$$

where N is the number of spins and S is the spin quantum number ($S = \frac{1}{2}, 1, \dots$). Equation (4) generalizes the result derived by Wieśnał *et al.* [23] to the case of anisotropic g factor, relevant for surface spins [33], and constitutes the starting point to our proposed entanglement certification method. If the spin susceptibilities are measured, and violate the inequality of Eq. (4), the presence of entanglement is certified. Equation (4) is a *sufficient* condition for entanglement, but not necessary: entanglement may be present, but go unnoticed, if the susceptibility satisfies Eq. (4).

III. ENTANGLEMENT CERTIFICATION WITH ESR-STM

We discuss now how to certify entanglement using a single ESR-STM-active atom, that will be used as a sensor, placed nearby the spin array of interest. Specifically, we consider the case of dimers [34,35] and trimers [19] of antiferromagnetically coupled $S = 1/2$ spins on MgO [19], the canonical

surface for ESR-STM. The choice of $S = 1/2$ rules out single-ion anisotropies. In the Supplemental Material [30] we show how the role of dipolar interactions can be neglected in most cases. Examples of $S = 1/2$ adsorbates deposited on MgO include TiH [34–40], Cu [36], dimers of alkali atoms [41], and even organic molecules [42].

The spectra of the dimer and trimer are shown in Figs. 1(e) and 1(f) as a function of the applied field. The dimer shows a singlet ground state with wave function $\frac{1}{\sqrt{2}}(|\uparrow\downarrow\rangle - |\downarrow\uparrow\rangle)$ and a triplet of excited states ($S = 1, S_z$). The $S = 1, S_z = \pm 1$ are product states, whereas the $S = 1, S_z = 0$ are entangled. The trimer ground state is a $S = 1/2$ doublet with wave functions:

$$\left| \frac{1}{2}, +\frac{1}{2} \right\rangle = -\frac{1}{\sqrt{6}}(|\uparrow\uparrow\downarrow\rangle + |\downarrow\uparrow\uparrow\rangle) + \sqrt{\frac{2}{3}}|\uparrow\downarrow\uparrow\rangle \quad (5)$$

and an analogous formula for $|S = \frac{1}{2}, S_z = -\frac{1}{2}\rangle$. Therefore, both structures, dimer and trimer, have entangled ground states. The lowest energy excited state, with excitation energy J , is also a $S = 1/2$ doublet, whereas the highest energy multiplet has $S = 3/2$ and excitation energy $\frac{3J}{2}$.

Experiments [29] show that the ESR spectrum, i.e., the $I_{DC}(f)$ curve of the sensor adatom, under the influence of a nearby spin array, can be described by

$$I_{DC}(f) = \sum_n p_n L(f - f_n), \quad (6)$$

where the sum runs over the eigenstates of the Hamiltonian of the spin array, $(\mathcal{H}_0 + \mathcal{H}_1)|n\rangle = E_n|n\rangle$, and L is a Lorentzian curve centered around the resonant frequency $f = f_n$, given

by the expression

$$f_n(\vec{r}) = \frac{\mu_B}{h} \sqrt{\sum_{\alpha} \{g_{\alpha}^{\text{sensor}} [B_{\alpha} + b_{n,\alpha}(\vec{r})]\}^2}. \quad (7)$$

Here, $h = 2\pi\hbar$, $g_{\alpha}^{\text{sensor}}$ are the components of the gyromagnetic tensor of the sensor, B_{α} represents the external field, and $b_{n,\alpha}(\vec{r})$ is the α component of the stray field generated by the spin array in the state n . The vector is given by

$$\vec{b}_n(\vec{r}) = \frac{\mu_0}{4\pi} \sum_{i=1,N} \frac{3[\vec{m}^i(n) \cdot \vec{d}^i] \vec{d}^i}{(d^i)^5} - \frac{\vec{m}^i(n)}{(d^i)^3}, \quad (8)$$

where \vec{r}^i are the positions of the surface spins and \vec{r} is the position of the sensor, $\vec{d}^i = \vec{r} - \vec{r}^i$, and $\vec{m}^i(n)$ is a vector given with components by

$$m_{\alpha}^i(n) = -g_{\alpha} \mu_B \langle n | S_{\alpha}^i | n \rangle \quad (9)$$

that encode the quantum-average magnetization of the atomic moments of the spin array for state n . Equation (6) implicitly assumes the absence of resonant spin-flip interactions between the sensor spin and the spin array.

In Fig. 1(d) we show the spectra for a sensor nearby a dimer and a trimer of antiferromagnetically coupled spins, in the presence of an external field along the z direction, assuming a broadening $\Delta f = 5$ MHz [27]. The frequency shift of the n peak, with respect to the bare sensor, are governed by the stray field $\vec{b}_n(\vec{r})$ generated by that state. For the dimer, the ESR spectrum shows a prominent peak, that has contributions from both the $S = 0, S_z = 0$ and $S = 1, S_z = 0$ states, whose stray field vanishes. As a result, the prominent peak has the frequency of the bare sensor. The two smaller peaks, symmetrically located around the central peak, correspond to the $S = 1, S_z = \pm 1$ states. In the case of the trimer up to eight different peaks appear in our simulation, as the different doublets generate states with different magnetization and stray field.

We now express the average magnetization and the susceptibility in terms of the occupations p_n and the magnetic moment of each state, the two quantities that can be obtained from ESR-STM. For spin-rotational invariant systems, we write Eq. (1) as

$$\langle M_{\alpha} \rangle = \sum_n p_n M_{\alpha}(n), \quad (10)$$

where $p_n = \frac{1}{Z} e^{-\beta E_n}$ is the equilibrium occupation of the n eigenstate and $M_{\alpha}(n) = -g_{\alpha} \mu_B S_{\alpha}(n)$, and $S_{\alpha}(n)$ is the (half-)integer projection of the total spin operator of the spin array along the α direction. The susceptibility would be given by

$$\chi_{\alpha} = \sum_n \frac{d p_n}{d B_{\alpha}} M_{\alpha}(n). \quad (11)$$

The experimental protocol to determine the p_n is the following [29]. For an ESR spectrum with N_p visible peaks, we obtain the ratios $r_n = \frac{I_n}{I_0}$ where I_0 corresponds to the largest peak that arises from a single state. For trimers, I_0 is the peak that arises from the ground state. For dimers, the ground state peak also has contributions from the $S = 1, S_z = 0$ state and therefore

we normalize with respect to the $S = 1, S_z = -1$ peak. It has been demonstrated [29] that the ratio of thermal occupations is the same as the ratio of Boltzmann factors $r_n = \frac{p_n}{p_0} = \frac{I_n}{I_0}$. Assuming that the peaks exhaust the occupations of the states, we obtain p_n out of the ratios (see Supplemental Material [30]).

The determination of the $M_{\alpha}(n)$ can be done in two ways. First, the (half-)integer values of S_{α} could be assigned by inspection of the ESR spectrum relying on the fact that the states with largest S_{α} have larger stray field. We have verified [43] the feasibility of a second approach where the readout of the ESR spectra is repeated with the sensor in different locations, mapping the stray field of every state in real space, and pulling out the atomic magnetization averages, inferring $M_{\alpha}(n)$ thereby.

The protocol to measure the spin susceptibility of a spin array has the following steps, that have to be implemented for the three orientations $\alpha = x, y, z$ of the external field:

(1) The bare resonant frequencies for the sensor $f_{0\alpha} = \frac{\mu_B}{h} g_{\alpha}^{\text{sensor}} B_{\alpha}$ [Fig. 1(a)] are determined in the *absence* of the spin array.

(2) The g_{\min} for the individual spins that form the array are determined. If they are ESR-STM active, a conventional resonance experiment is carried out, for the three directions of the field. Otherwise, the nearby ESR-STM sensor atom can be used [29].

(3) The $M_{\alpha}(n)$ and p_n are obtained as explained above, for two values of $B_{\alpha}^{(1)}$ and $B_{\alpha}^{(2)}$. This permits us to obtain $\langle M_{\alpha}(B_{\alpha}^{(1)}) \rangle$ and $\langle M_{\alpha}(B_{\alpha}^{(2)}) \rangle$ for both fields and $\chi_{\alpha} = \frac{\langle M_{\alpha}(B_{\alpha}^{(2)}) \rangle - \langle M_{\alpha}(B_{\alpha}^{(1)}) \rangle}{B_{\alpha}^{(2)} - B_{\alpha}^{(1)}}$ and compare to Eq. (4) to establish the presence of entanglement.

IV. RESULTS

In the top panels of Fig. 2, we show the spin susceptibility for dimers and trimers as a function of temperature, together with the EW boundary, assuming isotropic factors, $g_{\alpha} = 2$. We define the temperature T^* , below which the trace of the susceptibility matrix is smaller than the entanglement witness limit, so that Eq. (4) is not satisfied, and therefore the presence of entanglement is certified. The $\text{Tr} \chi(T)$ curves are very different for dimer and trimer. At low T , the dimer is in the singlet state and its susceptibility vanishes. In contrast, for the trimer with $J \gg k_B T$, the excited states play no role and the spin susceptibility is governed by the two states of the $S = 1/2$ ground state doublet.

The implementation of the entanglement certification protocol will only be possible if the stray fields induce a shift larger than the spectral resolution of ESR-STM. For ESR-STM, $\Delta f \simeq 4$ MHz [27], determined by the T_1, T_2 times of the adsorbate in that system. In the simulations of Fig. 1 we have used $\Delta f = 5$ MHz. In addition, the experiment has to meet four experimental conditions.

Condition I: temperature T has to be smaller than T^* .

Condition II: $M_{\alpha}(B_{\alpha})$ has to be linear. We define B^* as the upper value of the field above which $\frac{dM_{\alpha}}{dB_{\alpha}}$ deviates from its value for $B = 0$ more than 5%.

Condition III: the relative error in the current of the reference peak $\frac{\Delta I}{I_0}$ should be small enough to allow for the accurate

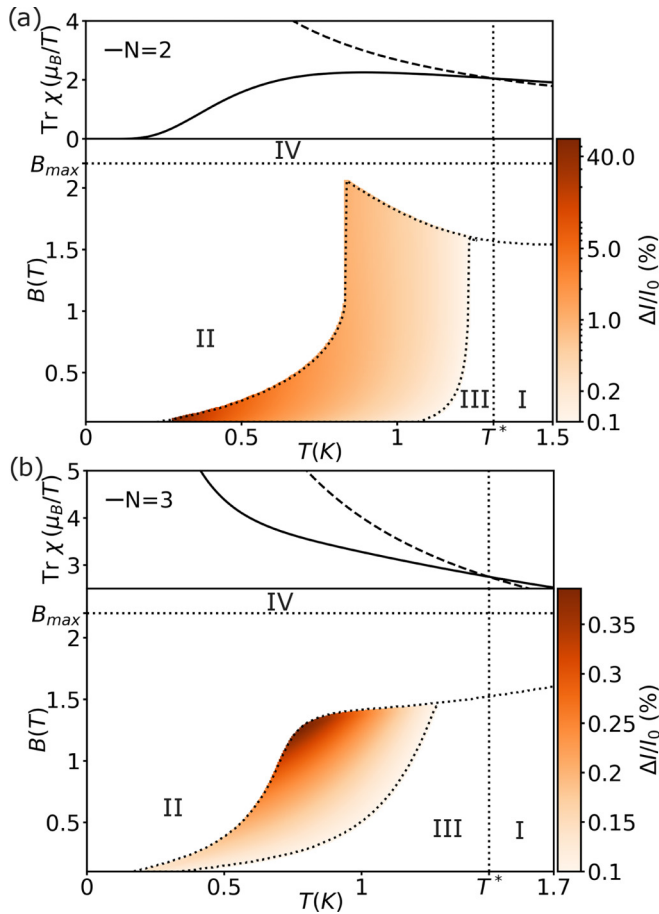


FIG. 2. Entanglement certification window (see text) for a dimer (a) and trimer (b) with $J = 124 \mu\text{eV}$, using a sensor located 0.9 nm away. Top panels show $\text{Tr } \chi(T)$ and the EW condition of Eq. (4). Color map inside the ECWs represents the largest experimental error $\Delta I/I_0$ that still makes entanglement certification possible, assuming $\eta = 5$ in Eq. (12).

entanglement certification. Specifically, the error in the spin susceptibility associated to $\frac{\Delta I}{I_0}$, should be smaller, by a factor $\eta \gg 1$, than the difference between χ_α and the EW condition. In the Supplemental Material [30] we show this condition is

$$\frac{\Delta I}{I_0} < \frac{B|\text{Tr } \chi - \chi_{EW}|}{6\eta p_0 \sum_n ([2 + r_n + (N_p - 2)p_0]|M_\alpha(n)|)}. \quad (12)$$

Condition IV: the external field must not drive the sensor resonant frequency above the excitation bandwidth of ESR-STM. The record, so far, is $f_0 = 61 \text{ GHz}$ [35], which translates into $B \simeq 2.2 \text{ T}$ for $S = 1/2$ Ti-H adsorbates.

The independent satisfaction of conditions I–IV occurs only in a region of the (B, T) plane, defining four boundary lines, one per condition. We define the *entanglement certification window* (ECW) as the area where the four conditions are satisfied simultaneously. In Fig. 2 we show the ECW, assuming $\eta = 5$ and imposing for condition III that $\Delta I/I_0$ cannot go below 10^{-3} , for the case of a dimer (a) and a trimer (b) with the same J reported by Yang *et al.* [19], $J = 124 \mu\text{eV}$ (30 GHz). The color code signals the maximal $\Delta I/I_0$ that satisfies Eq. (12).

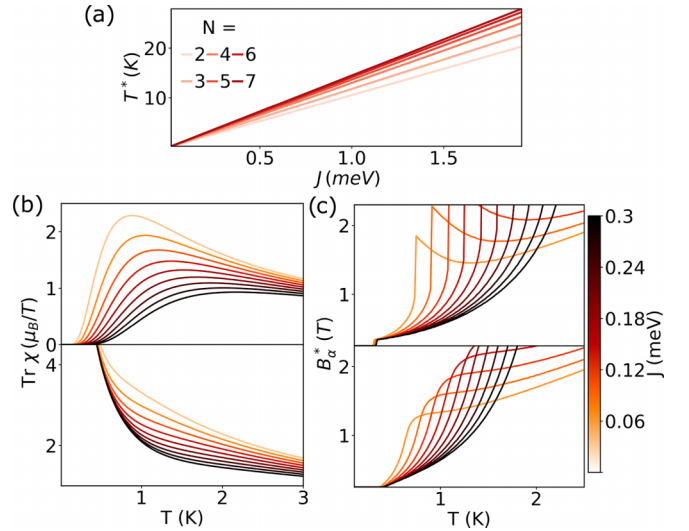


FIG. 3. (a) $T^*(J)$ for different chain sizes. (b),(c) Temperature and J dependence of the spin susceptibility (b) and B^* (c) of dimer (top) and trimer (bottom).

We now discuss the effect of the value of J on the size of the ECW. In Fig. 3(a) we show that T^* is strictly linear with J for spin chains with N sites, and the slope is an increasing function of the number of N . Therefore, both long chains and large J increase the crossover temperature. As of condition II, our numerical simulations show that B^* is an increasing function of both T and J : the magnetization vs field curves remain linear as long as the Zeeman energy is smaller than the other two relevant energy scales J and T . Condition III is governed both by the ratio $B/p_0(B, T)$ [see Eq. (12)] and by the susceptibility. In Fig. 3(b) we show the J dependence of the $\chi(T)$ curves. We see that reducing J tends to increase χ , at a fixed value of T . Again, this reflects the competition between exchange and Zeeman energies. Therefore, increasing J pushes T^* up and pushes the $\chi(T)$ away from the EW boundary. The only advantage of smaller values of $J/K_B T$ is the presence of more peaks in the $I(f)$ spectra that makes the spectra clearly distinguishable from simpler structures.

V. CONCLUSIONS

In conclusion, we propose a method to determine the presence of quantum entanglement in on-surface spin arrays using ESR-STM, and circumventing the lack of single-shot spin readout that would give full access to the quantum states. For that matter, the trace of the spin susceptibility of the spin arrays has to be measured taking advantage of the STM potential (i) to manipulate atoms and build spin structures, and (ii) to simultaneously resolve the stray fields and occupation probabilities of several quantum states of nearby spins [29]. Our calculations show that the experiments can be carried out with the state-of-the-art ESR-STM instrumentation in terms of both spectral resolution (Δf) and relative error in the current $\Delta I/I_0$ [29]. The use of STM to certify the presence of entanglement would thus add another functionality to this versatile tool and would open another venue in quantum nanoscience [10].

ACKNOWLEDGMENTS

We acknowledge Antonio Costa for useful discussions. J.F.R. acknowledges financial support from FCT (Grant No. PTDC/FIS-MAC/2045/2021), SNF Sinergia (Grant Pimag), FEDER/Junta de Andalucía, (Grant No. P18-FR-4834),

Generalitat Valenciana funding Prometeo2021/017 and MFA/2022/045, and funding from MICINN-Spain (Grant No. PID2019-109539GB-C41). Y.D.C. acknowledges funding from FCT and QPI, (Grant No. SFRH/BD/151311/2021) and acknowledges the hospitality of the Departamento de Física Aplicada at the Universidad de Alicante.

- [1] J. S. Bell, *Speakable and Unspeakable in Quantum Mechanics: Collected Papers on Quantum Philosophy* (Cambridge University Press, Cambridge, UK, 2004).
- [2] C. H. Bennett, G. Brassard, C. Crépeau, R. Jozsa, A. Peres, and W. K. Wootters, *Phys. Rev. Lett.* **70**, 1895 (1993).
- [3] D. Bouwmeester, J.-W. Pan, K. Mattle, M. Eibl, H. Weinfurter, and A. Zeilinger, *Nature (London)* **390**, 575 (1997).
- [4] D. Boschi, S. Branca, F. De Martini, L. Hardy, and S. Popescu, *Phys. Rev. Lett.* **80**, 1121 (1998).
- [5] A. Kitaev and J. Preskill, *Phys. Rev. Lett.* **96**, 110404 (2006).
- [6] M. A. Nielsen and I. Chuang, *Quantum Computation and Quantum Information* (Cambridge University Press, 2002).
- [7] C. L. Degen, F. Reinhard, and P. Cappellaro, *Rev. Mod. Phys.* **89**, 035002 (2017).
- [8] W. K. Wootters, *Philos. Trans. R. Soc. A* **356**, 1717 (1998).
- [9] N. Friis, G. Vitagliano, M. Malik, and M. Huber, *Nat. Rev. Phys.* **1**, 72 (2019).
- [10] A. J. Heinrich, W. D. Oliver, L. M. Vandersypen, A. Ardavan, R. Sessoli, D. Loss, A. B. Jayich, J. Fernandez-Rossier, A. Laucht, and A. Morello, *Nat. Nanotechnol.* **16**, 1318 (2021).
- [11] M. C. Arnesen, S. Bose, and V. Vedral, *Phys. Rev. Lett.* **87**, 017901 (2001).
- [12] L. Amico and R. Fazio, *J. Phys. A: Math. Theor.* **42**, 504001 (2009).
- [13] C. F. Hirjibehedin, C. P. Lutz, and A. J. Heinrich, *Science* **312**, 1021 (2006).
- [14] A. A. Khajetoorians, D. Wegner, A. F. Otte, and I. Swart, *Nat. Rev. Phys.* **1**, 703 (2019).
- [15] D.-J. Choi, N. Lorente, J. Wiebe, K. von Bergmann, A. F. Otte, and A. J. Heinrich, *Rev. Mod. Phys.* **91**, 041001 (2019).
- [16] F. Delgado and J. Fernández-Rossier, *Prog. Surf. Sci.* **92**, 40 (2017).
- [17] Y. Chen, Y. Bae, and A. J. Heinrich, *Adv. Mater.* **35**, 2107534 (2022).
- [18] S. Mishra, G. Catarina, F. Wu, R. Ortiz, D. Jacob, K. Eimre, J. Ma, C. A. Pignedoli, X. Feng, P. Ruffieux, J. Fernandez-Rossier, and R. Fasel, *Nature (London)* **598**, 287 (2021).
- [19] K. Yang, S.-H. Phark, Y. Bae, T. Esat, P. Willke, A. Ardavan, A. J. Heinrich, and C. P. Lutz, *Nat. Commun.* **12**, 1 (2021).
- [20] R. Toskovic, R. Van Den Berg, A. Spinelli, I. Eliens, B. Van Den Toorn, B. Bryant, J.-S. Caux, and A. Otte, *Nat. Phys.* **12**, 656 (2016).
- [21] J. Elzerman, R. Hanson, L. Willems van Beveren, B. Witkamp, L. Vandersypen, and L. P. Kouwenhoven, *Nature (London)* **430**, 431 (2004).
- [22] P. Neumann, J. Beck, M. Steiner, F. Rempp, H. Fedder, P. R. Hemmer, J. Wrachtrup, and F. Jelezko, *Science* **329**, 542 (2010).
- [23] M. Wieśniak, V. Vedral, and Č. Brukner, *New J. Phys.* **7**, 258 (2005).
- [24] Č. Brukner, V. Vedral, and A. Zeilinger, *Phys. Rev. A* **73**, 012110 (2006).
- [25] V. Vedral, *Nature (London)* **453**, 1004 (2008).
- [26] S. Sähling, G. Remenyi, C. Paulsen, P. Monceau, V. Saligrama, C. Marin, A. Revcolevschi, L. Regnault, S. Raymond, and J. Lorenzo, *Nat. Phys.* **11**, 255 (2015).
- [27] S. Baumann, W. Paul, T. Choi, C. P. Lutz, A. Ardavan, and A. J. Heinrich, *Science* **350**, 417 (2015).
- [28] F. D. Natterer, K. Yang, W. Paul, P. Willke, T. Choi, T. Greber, A. J. Heinrich, and C. P. Lutz, *Nature (London)* **543**, 226 (2017).
- [29] T. Choi, W. Paul, S. Rolf-Pissarczyk, A. J. Macdonald, F. D. Natterer, K. Yang, P. Willke, C. P. Lutz, and A. J. Heinrich, *Nat. Nanotechnol.* **12**, 420 (2017).
- [30] See Supplemental Material at <http://link.aps.org/supplemental/10.1103/PhysRevB.108.115413> for a derivation of Eq. (3); the role of dipolar interactions in spin susceptibility; obtaining thermal occupations from current peak ratios; and the relative error in the current peaks to certify entanglement. It also contains Ref. [31].
- [31] S. Ghosh, T. Rosenbaum, G. Aeppli, and S. Coppersmith, *Nature (London)* **425**, 48 (2003).
- [32] H. F. Hofmann and S. Takeuchi, *Phys. Rev. A* **68**, 032103 (2003).
- [33] A. Ferrón, S. A. Rodríguez, S. S. Gómez, J. L. Lado, and J. Fernández-Rossier, *Phys. Rev. Res.* **1**, 033185 (2019).
- [34] K. Yang, Y. Bae, W. Paul, F. D. Natterer, P. Willke, J. L. Lado, A. Ferrón, T. Choi, J. Fernández-Rossier, A. J. Heinrich *et al.*, *Phys. Rev. Lett.* **119**, 227206 (2017).
- [35] P. Kot, M. Ismail, R. Drost, J. Siebrecht, H. Huang, and C. R. Ast, [arXiv:2209.10969](https://arxiv.org/abs/2209.10969).
- [36] K. Yang, P. Willke, Y. Bae, A. Ferrón, J. L. Lado, A. Ardavan, J. Fernández-Rossier, A. J. Heinrich, and C. P. Lutz, *Nat. Nanotechnol.* **13**, 1120 (2018).
- [37] K. Yang, W. Paul, F. D. Natterer, J. L. Lado, Y. Bae, P. Willke, T. Choi, A. Ferrón, J. Fernández-Rossier, A. J. Heinrich *et al.*, *Phys. Rev. Lett.* **122**, 227203 (2019).
- [38] T. S. Seifert, S. Kovarik, D. M. Juraschek, N. A. Spaldin, P. Gambardella, and S. Stepanow, *Sci. Adv.* **6**, eabc5511 (2020).
- [39] M. Steinbrecher, W. M. J. van Weerdenburg, E. F. Walraven, N. P. E. van Mullekom, J. W. Gerritsen, F. D. Natterer, D. I. Badrtdinov, A. N. Rudenko, V. V. Mazurenko, M. I. Katsnelson, A. van der Avoird, G. C. Groenenboom, and A. A. Khajetoorians, *Phys. Rev. B* **103**, 155405 (2021).
- [40] L. M. Veldman, L. Farinacci, R. Rejali, R. Broekhoven, J. Gobeil, D. Coffey, M. Ternes, and A. F. Otte, *Science* **372**, 964 (2021).
- [41] S. Kovarik, R. Robles, R. Schlitz, T. S. Seifert, N. Lorente, P. Gambardella, and S. Stepanow, *Nano Lett.* **22**, 4176 (2022).
- [42] C. Lutz, G. Czap, and M. Sherwood, *Bull. Am. Phys. Soc.* **67** (2022).
- [43] Y. del Castillo and J. Fernández-Rossier (unpublished).